



High performance visible-light responsive Chl-Cu/ZnO catalysts for photodegradation of rhodamine B



Chayet Worathitanon^{a,b}, Kuntida Jangyubol^{a,b}, Preeyaporn Ruengrung^{a,b}, Waleeporn Donphai^{a,b}, Wantana Klysubun^c, Narong Chanlek^c, Phatthanon Prasitchoke^d, Metta Chareonpanich^{a,b,*}

^a KU-Green Catalysts Group, Department of Chemical Engineering, Faculty of Engineering, Kasetsart University, Bangkok 10900, Thailand

^b Nanocatalysts and Nanomaterials for Sustainable Energy and Environment Research Network of NANOTEC, Kasetsart University, Bangkok 10900, Thailand

^c Synchrotron Light Research Institute, Nakhon Ratchasima 30000, Thailand

^d PTT Global Chemical Public Company Limited, Bangkok 10900, Thailand

ARTICLE INFO

Keywords:

Chlorophyll
Cu/ZnO
RhB degradation
Visible light
Green catalyst

ABSTRACT

The photocatalytic degradation of rhodamine B (RhB) over chlorophyll-Cu co-modified ZnO catalysts (Chl-Cu/ZnO) was studied under visible-light irradiation. It was found that chlorophyll as an electron donor and copper in Cu²⁺ form help inhibit the recombination of electron-hole pairs and improve photoactivity of the catalyst. The synergistic effect between chlorophyll and Cu was found to improve visible-light response of ZnO nanoparticles, resulting in excellent performance in photodegradation of RhB. The appropriate ratio of chlorophyll and Cu loadings over ZnO was 0.5Chl-0.10Cu/ZnO—at this ratio, under visible-light irradiation of 2 h, the degradation efficiency was approximately 99% (60 mg/l of RhB solution), of which 18% of RhB adsorption occurred in dark condition. Moreover, outstanding reusability of Chl-Cu/ZnO, for up to six cycles, was found, with more than 80% degradation efficiency.

1. Introduction

Organic dyes are one of the main pollutants in wastewater released from food, textile, plastic and cosmetic industries. Even though the residual dyes in wastewater are present in low concentrations, they are still harmful to plants, aquatic animals and humans due to their non-biodegradable properties and toxicity [1–3]. Therefore, removal of dyes from wastewater is an essential process to lessen this environmental concern. To find out an appropriate solution, various techniques, including photocatalytic degradation [4], Fenton process [5], bioremediation [6] and ozonation [7], have been proposed. Among these techniques, catalytic photodegradation is considered as a potential method as it can be operated without expensive oxidants at low pressure and temperature using stable and low-cost catalysts [8–10]. In order to examine the degradation on efficiencies of photocatalysts, rhodamine B (RhB) is generally used as a representative dye since it is important in reference to its harmful impacts for human health, such as cancer, skin irritation, and allergic dermatitis [11–13].

Among various kinds of photocatalysts, zinc oxide (ZnO) and titanium dioxide (TiO₂) have been widely used for photodegradation [14–16] due to their non-toxicity, excellent thermal and chemical

stability and high photocatalytic efficiency [17,18]. In comparison to TiO₂, ZnO has received much attention because of its strong oxidation activity, low cost and high quantum efficiency [19,20]. However, due to the fact that the band-gap energy for visible-light activation is approximately 1.8–3.1 eV, ZnO, with its wide band-gap energy (3.3 eV), can be activated only under UV irradiation [21–23]. Taking inspiration from natural photosynthesis, chlorophyll, which plays a potential role as a photopigment, has been applied in the catalytic field to reduce the band-gap energy for photocatalytic applications under visible-light irradiation. Phongamwong et al. [24] used chlorophyll in *Spirulina* with N-doped TiO₂ for CO₂ reduction and found that chlorophyll could improve the photocatalytic activity under visible-light irradiation by acting as a sensitizer and electron donor, effectively giving an electron for promoting photoreaction. In addition, chlorophyll has also been found to promote the degradation of adsorbed dye molecules by facilitating the absorption of dye and thus leading to better photocatalytic ability [25,26].

In order to improve ZnO based catalysts in terms of the vital problems that are the recombination of electron-hole ($e^- - h^+$) pairs and backward reaction [27,28], metals such as Fe, Ag, Ni and Cu have been doped onto ZnO [29–31]. Among these, Cu is promising in the

* Corresponding author at: KU-Green Catalysts Group, Department of Chemical Engineering, Faculty of Engineering, Kasetsart University, Bangkok 10900, Thailand.

E-mail address: fengmtc@ku.ac.th (M. Chareonpanich).

prevention of the formation of recombination centers [32–34] as it can potentially substitute zinc atoms in ZnO lattice because of the similar size of ionic radius of Cu and Zn. Moreover, copper can improve photocatalytic activity of ZnO by providing electron capture to separate charges [35,36]. In addition, the strong coupling interaction between O 2p and Cu 3d plays an important role in narrowing the band-gap energy in Cu/ZnO system, resulting in visible-light activation ability [37].

In this work, a series of chlorophyll-Cu co-modified ZnO (Chl-Cu/ZnO) catalysts were synthesized and investigated for photocatalytic degradation of rhodamine B under visible-light irradiation. Outstanding performances of Chl-Cu/ZnO catalysts, particularly in terms of high catalytic activity under visible-light irradiation, were clearly observed due to the high capacity for dye adsorption and the inhibition potential of electron-hole pairs recombination.

2. Experimental

2.1. Preparation of chlorophyll-Cu co-modified catalysts

2.1.1. Synthesis of ZnO nanoparticles

ZnO nanoparticles were synthesized through a low-temperature precipitation technique modified from the work reported by Akir et al. [38]. In this work, zinc acetate dihydrate ($\text{Zn}(\text{CH}_3\text{COO})_2 \cdot 2\text{H}_2\text{O}$: Loba) was used as a ZnO precursor, and deionized water was used as a solvent. A certain amount of sodium hydroxide (NaOH: PanReac AppliChem) was dissolved in deionized water and added dropwise into zinc acetate dehydrate solution at 60 °C; then the mixture was vigorously stirred for 2 h. After that, the mixture was centrifuged at 8000 rpm for 5 min to separate ZnO powder from the mixture. The obtained powder was washed several times with ethanol and dried at 60 °C for 12 h, and a white powder of ZnO nanoparticles was obtained.

2.1.2. Loading of copper onto ZnO catalyst

CuO was loaded onto ZnO catalysts by using an incipient wetness impregnation. A certain amount of copper nitrate trihydrate ($\text{Cu}(\text{NO}_3)_2 \cdot 3\text{H}_2\text{O}$: PanReac AppliChem, 98% purity), a copper precursor, was mixed with deionized water and added onto ZnO powder. The mixture was then vigorously stirred at 60 °C for 1 h and dried at 60 °C for 12 h. A soft-blue powder catalyst was obtained. The copper concentrations based on ZnO in the catalyst used in this series of experiments were 0.01, 0.05, 0.10, 0.15 and 0.20 wt.% Cu.

2.1.3. Preparation of chlorophyll-modified Cu/ZnO catalyst

Chlorophyll was loaded onto Cu/ZnO catalysts by incipient wetness impregnation. Firstly, dried *Spirulina* pellets were ground and dissolved with a certain amount of methanol at 70 °C for 2 min. The chlorophyll solution was centrifuged at 3500 rpm for 5 min to collect a supernatant solution. The loading amount of chlorophyll a can be calculated by Eq. (1) [39] as follows:

$$\text{Chlorophyll a (Chl a)} = 13.9A_{665} - 13.9A_{665} \quad (1)$$

where A_{665} is absorbance at 665 nm measured by using UV-vis spectrophotometer.

A certain volume of chlorophyll solution was added onto ZnO and Cu/ZnO catalysts, and the obtained mixture was stirred at 40 °C overnight until methanol had completely evaporated. The chlorophyll concentrations based on ZnO in the catalyst were 0.1, 0.5 and 1.0 wt.% Chl a.

2.2. Textural and chemical properties of chlorophyll-modified catalysts

The surface area and pore size distribution of chlorophyll-modified catalysts were examined by N_2 physisorption using a 3 Flex Surface Characterization Analyzer and calculated using the Brunauer–Emmett–Teller (BET) and Barrett–Joyner–Halenda methods

under relative pressure (P/P_0) at –196 °C. Specific pore volumes were obtained from adsorption data at a relative pressure of 0.995.

The morphology and chemical element mapping of all catalysts were analyzed by using a field emission scanning electron microscope (FE-SEM: JEOL, JSM-7600 F) equipped with an energy dispersive X-ray spectroscope (EDS: OXFORD, X-Max^N) operated at 15 keV with Pt-coated samples.

The crystal structure of catalysts was investigated by an X-ray diffraction (XRD) spectrometer (Bruker D8 Advance) operated with a Cu-K α radiation source at room temperature in the 2θ range of 5–70°, and crystallite size was analyzed by using the Scherrer equation.

The functional groups of catalysts were analyzed by using a Fourier Transform Infrared Spectrometer (FT-IR: Bruker TENSOR 27) connected with a DTGS detector and operated in the range of 4000–400 cm^{-1} .

X-ray photoelectron spectroscope (XPS), operated at Beamline 5.3 of the Synchrotron Light Research Institute (SLRI), Thailand, was used to analyze the chemical states and surface atomic concentrations of the catalysts. The maximum photon energy was set at 650 eV, and an energy step of 0.1 eV was used. The C 1s peak at 284.8 eV was applied as a reference peak to calibrate the binding energy.

X-ray absorption near edge structure (XANES) at Beamline 8 of the SLRI, Thailand, was used to examine the electronic state and band structure of Cu. Cu K-edge spectra were collected in fluorescence mode at room temperature by using a double crystal Beryl (1010) monochromator as the photon energy selection. To improve the signal of the spectra, four data scans (~3 h per scan) were applied and analyzed by the Athena program.

2.3. Optical properties and band-gap energy of chlorophyll-modified catalysts

UV-vis diffuse reflectance spectrometer (UV-vis DRS: JASCO, V-670) was used to examine the optical properties and band-gap energy of the catalysts using BaSO_4 as a reflectance standard. The Tauc plots and the Kubelka–Munk function were applied to calculate the band-gap energy.

Photoluminescence spectrometer (PL: AvaSpec-2048TEC, Avantes) operated in the range of 300–700 nm was used to analyze the inhibition of electron-hole pairs recombination and charge transfer of the catalysts. The excitation wavelength was set at 345 nm.

2.4. Photocatalytic degradation measurements

The photocatalytic performances of Chl-Cu/ZnO catalysts were evaluated via photocatalytic degradation of rhodamine B ($\text{C}_{28}\text{H}_{31}\text{ClN}_2\text{O}_3$: HIMEDIA). In each experiment, 30 mg of photocatalyst was mixed with 30 ml of RhB solution (60 mg/L) and continuously stirred in a glass tube reactor for 120 min. Under dark condition, oxygen gas was filled into the reactor for 30 min to achieve the adsorption–desorption equilibrium. After that, the concentration of RhB was measured, giving what is denoted the initial concentration (C_0). LED floodlights (NULITE: 2 bulbs total, 50 W each) located on opposite sides of the glass reactor were used as light sources to achieve the photocatalytic activation at a light intensity of $5.86 \pm 0.04 \text{ mW cm}^{-2}$ ($\lambda > 400 \text{ nm}$). At certain time intervals, samples were taken for further analysis. To measure the residual concentration of RhB, the supernatant solutions were analyzed with a UV-vis spectrophotometer (Thermo Scientific, Genesys 10 series) at a wavelength of 554 nm.

3. Results and discussion

3.1. Performance of chlorophyll-modified ZnO catalysts

As shown in Fig. 1, dye adsorption capacities over Chl/ZnO catalysts were significantly higher than that on the ZnO catalyst. The degradation of RhB was found to increase with increased loading of chlorophyll,

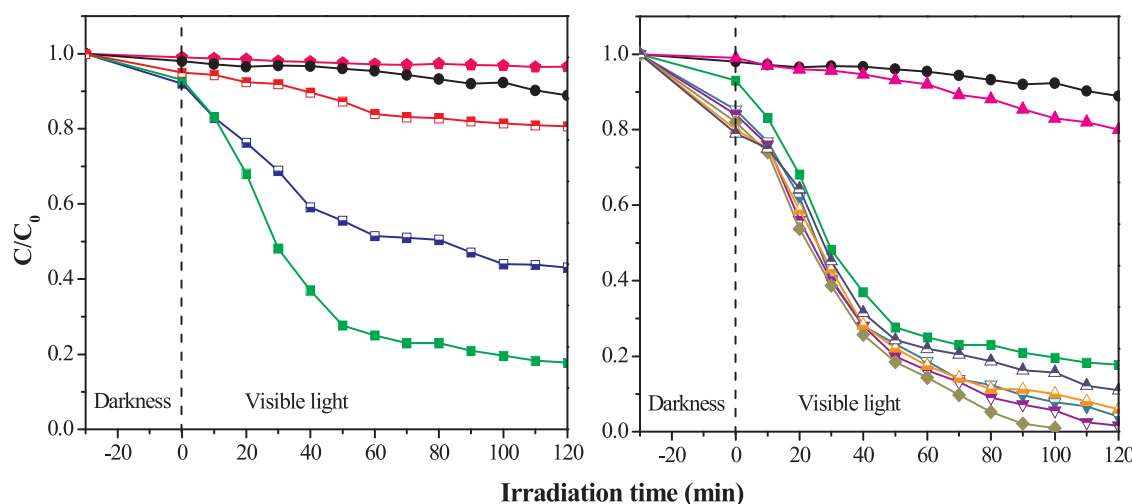


Fig. 1. Photocatalytic degradation of rhodamine B over modified ZnO and ZnO catalysts ($\text{RhB} = 60 \text{ mg/L}$).

—●— Photolysis, —●— ZnO, —□— 0.1Chl/ZnO, —■— 0.5Chl/ZnO, —■— 1.0Chl/ZnO, —▲— 0.1Cu/ZnO, —▼— 0.5Chl-0.01Cu/ZnO, —▼— 0.5Chl-0.05Cu/ZnO, —◆— 0.5Chl-0.10Cu/ZnO, —△— 0.5Chl-0.15Cu/ZnO, —△— 0.5Chl-0.20Cu/ZnO.

Table 1
Kinetic rate constant (k), regression coefficient (R^2) and percentage degradation of RhB under visible-light irradiation.

Catalysts	$K (10^{-3} \text{ min}^{-1})$	R^2	Degradation of RhB (%)
None	0.20	0.863	3.50
ZnO	0.80	0.935	11.1
0.1Chl/ZnO	10.6 ^a	0.962	56.9
0.5Chl/ZnO	41.2 ^a	0.965	82.9
1.0Chl/ZnO	1.77 ^a	0.943	19.3
0.1Cu/ZnO	1.80	0.973	20.0
0.5Chl-0.01Cu/ZnO	25.4	0.988	96.0
0.5Chl-0.05Cu/ZnO	29.3	0.983	98.4
0.5Chl-0.10Cu/ZnO	43.3	0.958	99.0
0.5Chl-0.15Cu/ZnO	22.4	0.975	94.0
0.5Chl-0.20Cu/ZnO	17.7	0.944	89.0

^a Second-order kinetic rate constant ($10^{-3} \text{ L mg}^{-1} \text{ min}^{-1}$).

such that the optimum chlorophyll loading, giving the best degradation efficiency among all Chl/ZnO catalysts was found to be 0.5 wt.% Chl a. At loading amounts higher than 0.5 wt.% Chl a, the degradation activity tended to decrease due to significant decreases in the specific surface areas of catalysts caused by chlorophyll blockages, as shown in Table 2.

To further examine the effect of copper on photocatalytic activity, various concentrations of copper (0.01, 0.05, 0.10, 0.15 and 0.20 wt.% Cu) were loaded onto ZnO. Following this, chlorophyll was loaded (0.5 wt.% Chl a) to obtain the co-modified Chl-Cu/ZnO catalysts. As shown in Fig. 1, the dye adsorption amount over 0.1Cu/ZnO catalyst was approximately the same as that over ZnO catalyst. However, with the chlorophyll-modified catalyst (0.5Chl/ZnO), the dye adsorption amount increased with increasing amounts of copper loading. To explain this behavior, copper was proposed to act as electron acceptor and attract adsorbed dye molecules on the catalyst surface, as will be explained later.

The photocatalytic degradation efficiencies of Chl-Cu/ZnO catalysts were found to be in the following order: 0.5Chl-0.10Cu/ZnO > 0.5Chl-0.05Cu/ZnO > 0.5Chl-0.01Cu/ZnO > 0.5Chl-0.15Cu/ZnO > 0.5Chl-0.20Cu/ZnO. The 0.5Chl-0.10Cu/ZnO catalyst showed the best performance among all catalysts. This result confirmed that both chlorophyll and copper had important roles in photodegradation of RhB. Notably, under visible-light irradiation of 2 h, the efficiency of 0.5Chl-0.10Cu/ZnO catalyst was approximately 99%, of which 18% of RhB adsorption occurred in dark condition. The synergistic effect between chlorophyll and copper on the elevation of photocatalytic activity of ZnO catalyst was examined. It was found that the RhB degradation

efficiencies of 0.5Chl-0.10Cu/ZnO were 1.2, 4.9 and 8.9 times higher than 0.5Chl/ZnO, 0.1Cu/ZnO and ZnO catalysts, respectively.

The kinetic rate constants of RhB degradation in this work were calculated by a pseudo-first-order kinetic model [40,41] and second-order kinetic model [42], using the following equations:

$$\ln(C_0/C) = k_1 t \quad (2)$$

$$(1/C) - (1/C_0) = k_2 t \quad (3)$$

where C_0 and C (mg/L) are concentrations of RhB at initial and times t , respectively; k_1 (min^{-1}) is pseudo-first-order kinetic rate constant; t (min) is irradiation time; and k_2 ($\text{L mg}^{-1} \text{ min}^{-1}$) is second-order kinetic rate constant. The plots of $\ln(C_0/C)$ and $(1/C) - (1/C_0)$ on the ordinate axes for the pseudo-first-order kinetic model in Eq. (2) for ZnO, Cu/ZnO and Chl-Cu/ZnO catalysts and the second-order kinetic model in Eq. (3) for Chl/ZnO catalysts with irradiation times on the abscissa axes were used to calculate the kinetic rates by linear regression, respectively. Good fits to both kinetic models were observed. The regression coefficients (R^2) are shown in Table 1. It was found that the second-order kinetic model by Chl/ZnO catalysts gave higher R^2 values in comparison to those of the pseudo-first-order kinetic model. These results confirmed that the second-order kinetic model is better represented the

Table 2
Specific surface area, total pore volume, average pore size and band gap of modified ZnO and ZnO catalysts.

Catalysts	Specific surface area (m^2/g)	Total pore volume (cm^3/g)	Average pore size (nm)	Band gap (eV) ^a
ZnO	33	0.17	32.8	3.18
0.1Chl/ZnO	23	0.14	34.3	3.12
0.5Chl/ZnO	16	0.10	45.4	2.87
1.0Chl/ZnO	8	0.06	45.6	2.77
0.1Cu/ZnO	35	0.18	29.7	3.16
0.5Chl-0.01Cu/ZnO	14	0.11	36.4	2.84
0.5Chl-0.05Cu/ZnO	13	0.10	39.2	2.80
0.5Chl-0.10Cu/ZnO	10	0.09	44.6	2.77
0.5Chl-0.15Cu/ZnO	12	0.11	36.7	2.86
0.5Chl-0.20Cu/ZnO	13	0.10	40.3	2.89

^a Calculated from the Kubelka-Munk plot in Fig. S6.

kinetics of RhB degradation on chlorophyll-modified ZnO catalysts.

In Table 1, it can be seen that the highest degradation rate ($43.3 \times 10^{-3} \text{ min}^{-1}$) was obtained using 0.5Chl-0.10Cu/ZnO catalyst—a value which was 24 and 54 times higher than those of 0.1Cu/ZnO and ZnO catalysts, respectively.

Since the band-gap energy represents the energy required to promote electrons from the valence band to the conduction band of the photocatalyst, a catalyst with a lower band-gap energy implies better photocatalytic activity under visible-light irradiation. As shown in Table 2, the 0.5Chl-0.10Cu/ZnO catalyst with the lowest band-gap energy among all catalysts exhibited the best performance in photo-degradation, confirming the above.

Moreover, the significant decrease of PL intensity of the Chl-Cu/ZnO catalysts implied potential in the inhibition of electron-hole pairs recombination, resulting in more charges free to participate in the reaction and consequently outstanding RhB degradation.

In order to indicate the complete mineralization of RhB, the amount of CO₂ from photodegradation of RhB over 0.5Chl-0.10Cu/ZnO catalyst was analyzed by using a gas chromatograph (Shimadzu GC-2014). It was found that the CO₂ amount increased through a reaction time as shown in Fig. S1. This evidence clearly indicated the gradual degradation of RhB during the reaction time period of 120 min. The result of CO₂ formation was in good agreement with that of RhB degradation efficiency calculated from UV-vis spectrophotometer in Table 1.

3.2. Morphology and surface characteristics of modified ZnO catalysts

In order to clarify the roles of chlorophyll and copper loaded on ZnO catalyst in the improvement of the photocatalytic activity, the structural morphology and surface characteristics of modified ZnO catalysts were examined in detail. The XRD patterns of all modified ZnO catalysts (Fig. S2) present the existence of ZnO [43], with copper not being detected due to it being loaded only in small amounts.

In the FE-SEM images (Fig. S3), ZnO nanoparticles had spherical shapes for all catalysts (Fig. S3a–d). In the case of 0.5Chl-0.10Cu/ZnO, the catalyst was partially covered by chlorophyll, with a good dispersion of copper atoms being observed from the EDS mapping of Cu (Fig. S4).

N₂ adsorption-desorption analysis of all the catalysts (Fig. S5) confirmed the presence of a type IV isotherm with H1 hysteresis loop, indicating the existence of a mesoporous structure in the modified ZnO catalysts. In Table 2, it can be seen that the specific surface areas of the chlorophyll-modified ZnO catalysts decreased slightly when chlorophyll loading amounts were greater than 0.5%. This was due to partial coverage of chlorophyll, which may result in a decrease in photo-degradation performance of the catalysts. In addition, with copper loading onto the 0.5Chl/ZnO catalyst, the pore size of the obtained catalyst (0.5Chl-0.10Cu/ZnO) decreased.

The functional groups of ZnO and modified ZnO catalysts were analyzed by FT-IR spectroscope (Fig. 2). All the catalysts showed peaks at 437 and 3406 cm⁻¹, which correspond to Zn–O stretching of the tetrahedral structure of zinc atoms and O–H stretching, respectively. The existence of chlorophyll and nitrate ions, which had vital roles in RhB degradation, was also confirmed. In Fig. 2c and d, both the 0.5Chl/ZnO and 0.5Chl-0.10Cu/ZnO catalysts exhibited peaks of chlorophyll with C–H stretching of methyl or methylene group at 2920 cm⁻¹ and the conjugated ketone at 1632 cm⁻¹ [44,45]. In addition, NO₃⁻ ion asymmetric stretching was detected at 1385 cm⁻¹ [46] for 0.1Cu/ZnO and 0.5Chl-0.10Cu/ZnO catalysts (Fig. 2b and d) as there remained residual precursor of copper on the catalyst surface.

It should be mentioned here that, in addition to chlorophyll, which could promote the RhB degradation by facilitating an absorption of RhB as an electron donor to ZnO catalyst, the NO₃⁻ ion could also form hydroxyl radical (·OH) as one of the reactive oxygen species and therefore promote the RhB degradation [47]. Details regarding these aspects of the mechanism will be discussed in the following sections.

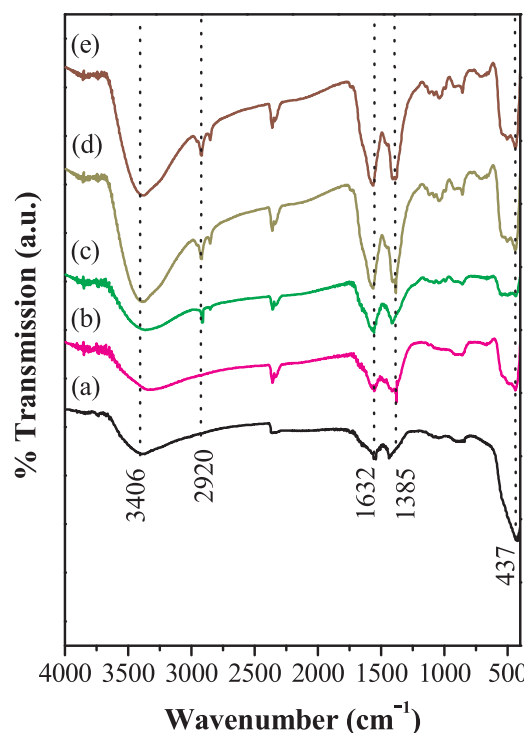


Fig. 2. FT-IR spectra of (a) ZnO, (b) 0.1Cu/ZnO, (c) 0.5Chl/ZnO, (d) 0.5Chl-0.10Cu/ZnO and (e) 0.5Chl-0.10Cu/ZnO (used) catalysts.

3.3. Chemical states of modified ZnO catalysts

XPS spectra of ZnO and modified ZnO catalysts in Fig. 3A include those of N 1s core level at 399.7 eV. This confirms the existence of porphyrin ring of nitrogen atoms around the magnesium atom of chlorophyll in 0.5Chl/ZnO and 0.5Chl-0.10Cu/ZnO catalysts [48] and thus the presence of chlorophyll on the catalyst surface. However, without chlorophyll loading, a broad peak of N 1s was observed, as can be seen in the cases of ZnO and 0.1Cu/ZnO catalysts. In Fig. 3B, the spectra of Cu 2p_{3/2} core level were detected at 933.4 and 933.5 eV in 0.1Cu/ZnO and 0.5Chl-0.10Cu/ZnO catalysts, respectively. These binding energies (between 933.6 and 934.1 eV) confirmed the oxidation state of copper in the form of Cu²⁺ [49].

The atomic ratios of each element were identified by calculating the atomic sensitivity factors of C 1s, Zn 2p, O 1s, N 1s and Cu 2p_{3/2} core levels and their photoemission areas. For copper, atomic ratios were 0.17 and 0.14 at.% for 0.1Cu/ZnO and 0.5Chl-0.10Cu/ZnO catalysts, respectively. This result clearly indicated that chlorophyll loading partially blocked the surface of catalysts and reduced the amount of surface copper to some extent.

In addition to the XPS results, the normalized Cu K-edge XANES spectra (Fig. 4) also revealed that the electronic state of copper both in the Cu-modified (0.1Cu/ZnO) and the chlorophyll-Cu co-modified catalysts (0.5Chl-0.10Cu/ZnO) was Cu²⁺, which was consistent to that of the copper precursor Cu(NO₃)₂.

3.4. Optical properties of modified ZnO catalysts

The absorption spectra of ZnO and modified ZnO catalysts obtained from UV-vis DRS are shown in Fig. 5. The absorption band of unmodified ZnO catalyst (Fig. 5a) at 400 nm indicates the visible-light response characteristics of this catalyst. With chlorophyll loading, the absorption spectra moved to 380–700 nm (Fig. 5b–d), representing the redshift due to a band-gap narrowing caused by the incorporation of chlorophyll onto the ZnO catalyst, as shown in Table 2. This phenomenon, implying the enhancement of visible-light activation potential,

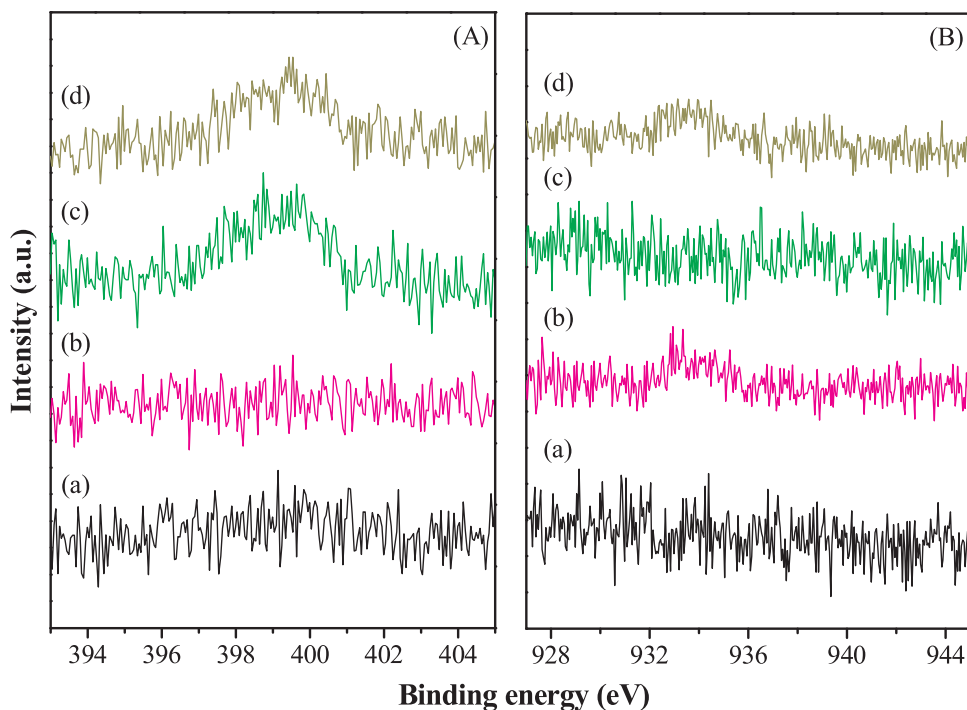


Fig. 3. High-resolution XPS spectra of (A) N 1s and (B) Cu 2p_{3/2} of (a) ZnO, (b) 0.1Cu/ZnO, (c) 0.5Chl/ZnO and (d) 0.5Chl-0.10Cu/ZnO catalysts.

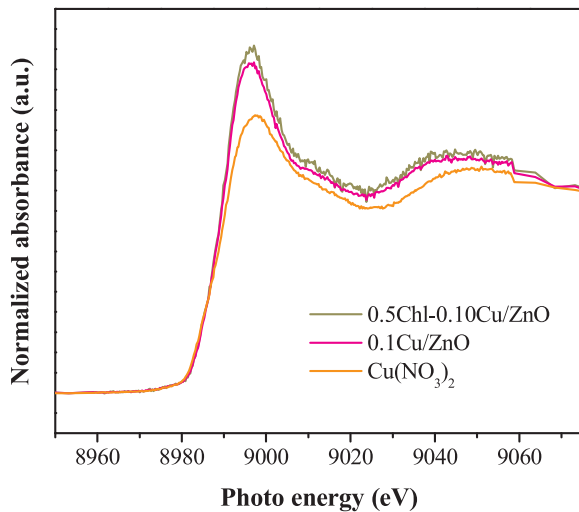


Fig. 4. Normalized Cu K-edge XANES spectra of 0.1Cu/ZnO, 0.5Chl-0.10Cu/ZnO catalysts and reference compound Cu(NO₃)₂.

resulted in the improvement of the RhB photodegradation efficiency.

A similar phenomenon to that obtained with the incorporation of chlorophyll was also observed with Cu loading—the Cu-modified ZnO catalyst likewise exhibited the redshift of absorption spectra, as indicated by the broad absorption band at 510–700 nm of 0.1Cu/ZnO (Fig. 5e). As a result, the co-loading of chlorophyll and copper onto the ZnO catalyst (Fig. 5f–j) led to the attainment of the narrowest band-gap and thus the greatest improvement in the absorption ability under visible-light irradiation.

The PL spectra of ZnO and modified ZnO catalysts are shown in Fig. 6. For all catalysts, two emission peaks were observed in the visible-light region: one at 383 nm and another at 487 nm, corresponding to the recombination of free exciton [50,51] and a photo-generated hole with an electron occupying the oxygen vacancy in ZnO [52], respectively. It can be seen that the PL intensities of Chl/ZnO catalysts (Fig. 6b–d) decreased with increasing chlorophyll loading

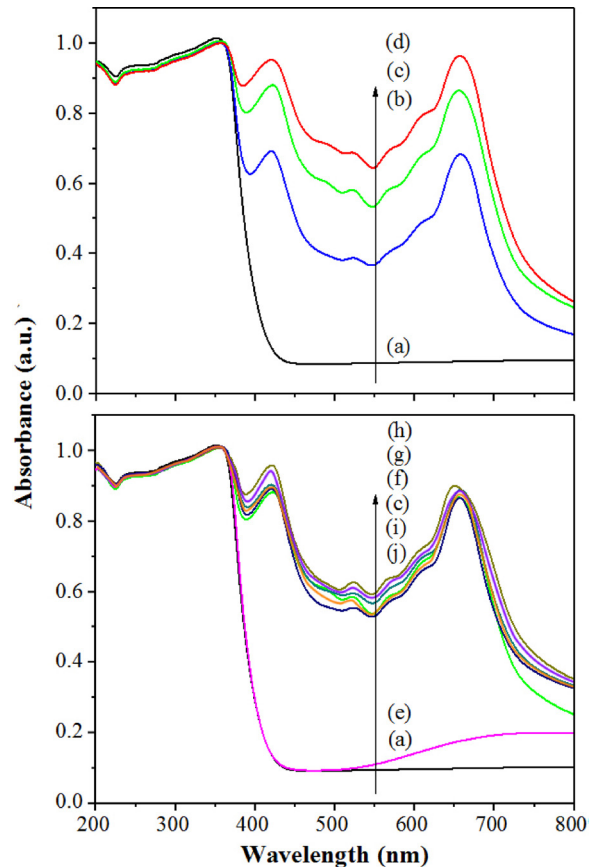


Fig. 5. UV-vis diffuse reflectance spectra of modified ZnO and ZnO catalysts: (a) ZnO, (b) 0.1Chl/ZnO, (c) 0.5Chl/ZnO, (d) 1.0Chl/ZnO, (e) 0.1Cu/ZnO, (f) 0.5Chl-0.01Cu/ZnO, (g) 0.5Chl-0.05Cu/ZnO, (h) 0.5Chl-0.10Cu/ZnO, (i) 0.5Chl-0.15Cu/ZnO and (j) 0.5Chl-0.20Cu/ZnO.

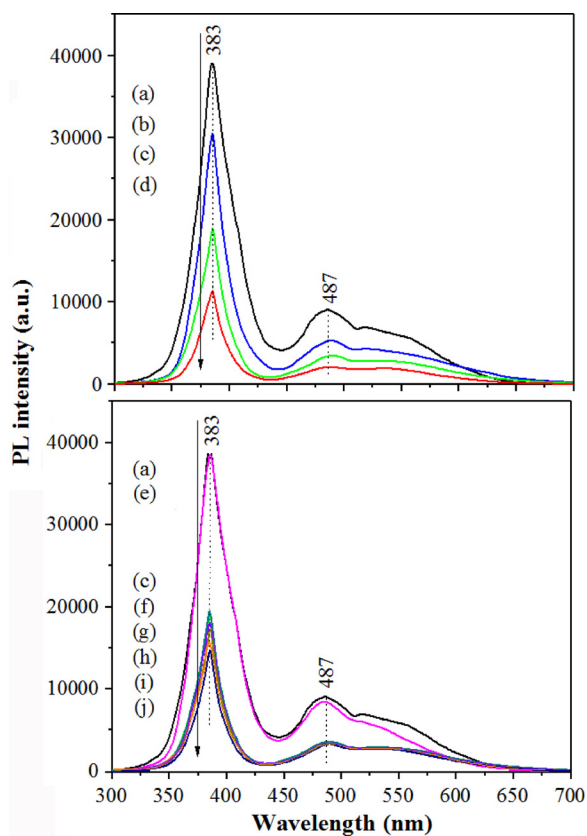


Fig. 6. PL spectra of modified ZnO and ZnO catalysts: (a) ZnO, (b) 0.1Chl/ZnO, (c) 0.5Chl/ZnO, (d) 1.0Chl/ZnO, (e) 0.1Cu/ZnO, (f) 0.5Chl-0.01Cu/ZnO, (g) 0.5Chl-0.05Cu/ZnO, (h) 0.5Chl-0.10Cu/ZnO, (i) 0.5Chl-0.15Cu/ZnO and (j) 0.5Chl-0.20Cu/ZnO.

amounts due to a charge transfer between chlorophyll and ZnO catalyst [53].

It should be noted that the PL intensity of 0.1Cu/ZnO catalyst (Fig. 6e) was quite similar to that of the ZnO catalyst. However, with the incorporation of chlorophyll (0.5Chl/ZnO catalyst), the increase of Cu loading could cause a gradual decrease in the PL intensities (Fig. 6f–j). As the PL intensity represents the recombination of free electrons and holes [54,55], the decrease in PL intensities by copper loading over the 0.5Chl/ZnO catalyst therefore indicated an outstanding inhibition of electron-hole pairs recombination, leading to excellent photodegradation performance. Moreover, it was found that a small amount of

copper loading could better restrain the recombination of photo-induced electron-hole pairs compared to a greater loading, as, in this latter case, the recombination centers could also be formed by the excess copper amounts.

As shown in Fig. 1, it was found that the RhB degradation efficiencies of 0.1Chl/ZnO, 0.5Chl/ZnO and 1.0Chl/ZnO were 5.1, 7.7, and 1.7 times higher than that of ZnO, respectively. Moreover, with chlorophyll loading onto ZnO catalysts, the absorption spectra moved to 380–700 nm (Fig. 5b–d). This result represented the redshift due to a band-gap narrowing, as shown in Table 2, implying the enhancement of visible-light activation potential and the improvement of the RhB photodegradation efficiency. In addition to the improvements in the RhB degradation efficiencies and band-gap narrowing, the PL intensities of Chl/ZnO catalysts decreased with increasing chlorophyll loading amounts (Fig. 6b–d). These results indicated an outstanding inhibition of electron-hole pairs recombination in comparison to that of ZnO (Fig. 6a) [54,55], leading to excellent photodegradation performance. Accordingly, it can be concluded that the photocatalytic activities over ZnO catalysts were significantly improved by the extracted chlorophyll on the ZnO surface which acted as an electron donor by transferring electrons to ZnO and improved the optical adsorption.

Moreover, after absorbing light energy, the electrons on chlorophyll moved to an excited state (singlet or triplet state), and then transferred to ZnO conduction band (CB) due to the energetically higher excited states of chlorophyll (−1.27 vs. SCE) than the conduction band of ZnO (−0.50 vs. SCE) [56,57]. This explanation confirmed the evidence of electron transfer from chlorophyll to ZnO.

Nonetheless, the higher loading amounts of chlorophyll (1.0 wt.% Chl a) on ZnO catalyst could lead to the lower RhB degradation performance compared to that of the 0.5Chl/ZnO catalyst. This was due to the formation of recombination center of the electron-hole pairs, as has been reported by Phongamwong et al. [24], and resulted in the decrease of photocatalytic activity of chlorophyll-modified ZnO catalyst.

3.5. Proposed mechanism of RhB photodegradation over Chl-Cu/ZnO catalyst

Based on the information regarding the structure and reactivity of the Chl-Cu/ZnO catalysts as mentioned in the previous sections, the mechanism of RhB degradation under visible-light irradiation (Fig. 7) was proposed as follows: Absorbing a photon from visible light, electrons are excited from a ground state of RhB to an excited state. Simultaneously, chlorophyll (Chl) absorbs photons from light, and electrons are promoted from a ground state to a singlet state ($^1\text{Chl}^*$). Some electrons move to a triplet state ($^3\text{Chl}^*$) by passing through an inter-system crossing (ISC) and then transfer to a conduction band of ZnO

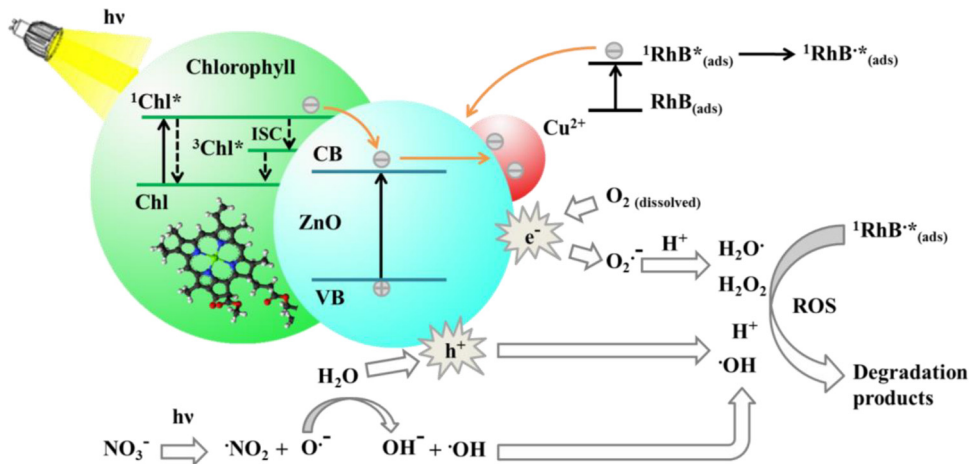


Fig. 7. Proposed mechanism for photocatalytic degradation of RhB on chlorophyll-Cu co-modified ZnO catalyst.

(CB). To regenerate back the cationic form of chlorophyll (Chl⁺) to the ground state (Chl), Chl⁺ receives electrons from an electron donor molecule through an electron carrier in the electron transport chain of *Spirulina* [58,59]. Simultaneously, electrons from ZnO move from the valence band (VB) to the conduction band (CB) but only when photon energy from visible light is greater than the band-gap energy of ZnO. On the ZnO surface, copper metals prevent electron-hole pairs recombination and act as trapping sites of electrons, facilitating the photodegradation of RhB [60,61]. In the conduction band of ZnO (CB), dissolved oxygen on the ZnO surface reacts with electrons to form superoxide radical (O₂^{·-}). In addition, the surface water reacts with holes in the valence band of ZnO (VB) to create reactive oxygen species (ROS). Due to the fact that the reactive oxygen species are highly-reductive radicals, RhB is consecutively degraded via the reaction with these reactive oxygen species under visible-light irradiation. In addition, the residual nitrate ion from copper nitrate dissolves in the RhB solution and dissociates into nitrogen dioxide and O^{·-} radical. This radical is then protonated with water to form hydroxyl ion and hydroxyl radical which consecutively degrade the residual dye [47].

In this research, the residual nitrate ion from copper nitrate was proposed to form hydroxyl ion and hydroxyl radical which then consecutively degraded the residual dye. Accordingly, the experiment was performed to clarify the proposed mechanism of nitrate ion by the nitrate-induced photodegradation of RhB. By using the same operating condition of RhB photodegradation over Chl-Cu/ZnO catalysts, 5 ml of sodium nitrate solution with different concentrations (1, 2, 3, 4 and 5 g/L) was mixed with 30 ml of RhB solution (60 mg/L) and continuously stirred in a glass tube reactor for 120 min. At certain time intervals, samples were taken for further analysis. To measure the residual concentration of RhB, the solution was analyzed by using a UV-vis spectrophotometer (Thermo Scientific, Genesys 10 series) at a wavelength of 554 nm. The photodegradation of RhB with sodium nitrate solutions is shown in Fig. S7.

As shown in Fig. S7, it was found that the degradation efficiency of RhB gradually increased from 2.5% to 7.5% with the increasing concentrations of sodium nitrate from 1 to 5 g/L. This result confirmed that the nitrate ion had an important role in RhB photodegradation by forming hydroxyl radical as one of the reactive oxygen species to degrade the dye [47].

3.6. Recyclability of Chl-Cu/ZnO catalyst

In practical applications, not only is the highly efficient photocatalytic degradation activity essential, but the reusability is also a key characteristic. To investigate the reusability of catalyst, the chlorophyll-copper co-modified catalyst which gave the highest photocatalytic degradation efficiency of RhB (0.5Chl-0.10Cu/ZnO) was tested in a cyclic photocatalytic experiment. As shown in Fig. 8, for all six cycles of photodegradation, more than 80% conversion was obtained, indicating stable efficiencies and steady dye adsorption. These results confirmed the excellent characteristics of 0.5Chl-0.10Cu/ZnO catalyst: its high activity, stability and recyclability. The positive change can be traced to the synergistic effect between chlorophyll and copper functioning as electron donor and acceptor on the surface of ZnO catalyst, respectively.

In addition, the used 0.5Chl-0.10Cu/ZnO catalyst was analyzed by FT-IR spectroscope and compared to that of the fresh catalyst (Fig. 2d and e) in order to investigate the change in functional groups after cyclic photocatalysis test. After six cycles of use, the FTIR peak corresponding to C-H stretching of methyl or methylene group (2920 cm⁻¹) was detected over the used catalyst, indicating the existence of chlorophyll on the catalyst. Moreover, the absence of the peak at 1385 cm⁻¹ (Fig. 2e) confirms the disappearance of NO₃⁻ ion from the catalyst surface by dissolution in the RhB solution and forming hydroxyl radical as one of the reactive oxygen species to degrade the residual dye [47].

Moreover, the amount of Chl deposited on ZnO after the

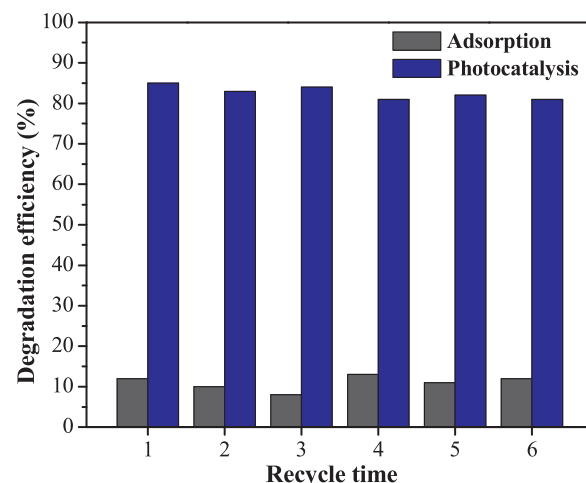


Fig. 8. Cycling run for the photocatalytic degradation of rhodamine B over 0.5Chl-0.10Cu/ZnO catalyst.

photocatalytic reaction was further evaluated. Due to the fact that Mg is the only metal in chlorophyll structure, the fresh 0.5Chl-0.10Cu/ZnO catalyst and the used catalyst after cyclic photocatalytic experiment were analyzed by using SEM-EDS to find Mg amounts. It was found that the amounts of Mg in the fresh and used catalysts were 0.09% (w/w) and 0.07% (w/w), respectively. These results indicated that approximately 80% of Mg from chlorophyll structure remained on the catalyst after six cycles of photodegradation.

4. Conclusion

Chlorophyll-Cu co-modified ZnO (Chl-Cu/ZnO) photocatalyst was successfully prepared and played a significant role in photodegradation of RhB under visible-light irradiation. Among all catalysts studied, chlorophyll-Cu co-modified ZnO catalyst gave the most outstanding degradation of RhB, attaining almost 99% within 2 h. The photocatalytic activities over ZnO catalysts were significantly improved by loadings of copper and the extracted chlorophyll on the ZnO surface. As an electron acceptor, copper in the Cu²⁺ form on the Cu/ZnO catalyst provided an inhibition of electron-hole recombination by capturing the excited electrons, enhancing the photodegradation by free holes on the valence band of ZnO. With Chl-Cu/ZnO catalysts, a synergistic effect between chlorophyll and Cu was observed—chlorophyll acted as an electron donor by transferring electrons to ZnO and improved the optical adsorption of Cu/ZnO, potentially promoting RhB degradation under visible-light irradiation. However, loading more chlorophyll and Cu than the optimum amounts (0.5 wt.% Chl a and 0.1 wt.% Cu) could lead to the decrease in photodegradation efficiency due to the formation of recombination centers of electron-hole pairs on the catalysts.

Acknowledgments

This work was financially supported by the Kasetsart University Research and Development Institute (KURDI), the Center of Excellence on Petrochemical and Materials Technology (PETROMAT), and the Institutional Research Grant (grant no. IRG5980004). The authors would like to thank the Synchrotron Light Research Institute (BL8: XAS and BL5.3: Nanotec-XPS) for their support regarding XAS and XPS measurements.

Appendix A. Supplementary data

Supplementary material related to this article can be found, in the online version, at doi:<https://doi.org/10.1016/j.apcatb.2018.09.048>.

References

[1] M. Karkmaz, E. Puzenat, C. Guillard, J.M. Herrmann, Photocatalytic degradation of the alimentary azo dye amaranth mineralization of the azo group to nitrogen, *Appl. Catal. B. Environ.* 51 (2004) 183–194.

[2] H. Lachheb, E. Puzenat, A. Houas, M. Ksibi, E. Elaloui, C. Guillard, J.-M. Herrmann, Photocatalytic degradation of various types of dyes (Alizarin S, Crocein Orange G, Methyl Red, Congo Red, Methylene Blue) in water by UV-irradiated titania, *Appl. Catal. B Environ.* 39 (2002) 75–90.

[3] H. Chen, J. Motuzas, W. Martens, J.C.D. da Costa, Degradation of azo dye Orange II under dark ambient conditions by calcium strontium copper perovskite, *Appl. Catal. B Environ.* 221 (2018) 691–700.

[4] Z. Xing, J. Zhang, J. Cui, J. Yin, T. Zhao, J. Kuang, Z. Xiu, N. Wan, Wei Zhou, Recent advances in floating TiO₂-based photocatalysts for environmental application, *Appl. Catal. B Environ.* 225 (2018) 452–467.

[5] L. Clarizia, D. Russo, I.D. Somma, R. Marotta, R. Andreozzi, Homogeneous photo-Fenton processes at near neutral pH: a review, *Appl. Catal. B Environ.* 209 (2017) 358–371.

[6] K. Vikrant, B.S. Giri, N. Raza, K. Roy, K.-H. Kim, B.N. Rai, R.S. Singh, Recent advancements in bioremediation of dye: current status and challenges, *Bioresour. Technol.* Rep. 253 (2018) 355–367.

[7] G. Moussavi, R. Khosravi, N.R. Omran, Development of an efficient catalyst from magnetite ore: characterization and catalytic potential in the ozonation of water toxic contaminants, *Appl. Catal. A Gen.* 445–446 (2012) 42–49.

[8] J. Qiu, X. Zhang, Y. Feng, X. Zhang, H. Wang, J. Yao, Modified metal-organic frameworks as photocatalysts, *Appl. Catal. B. Environ.* 231 (2018) 317–342.

[9] I.K. Konstantinou, T.A. Albanis, TiO₂-assisted photocatalytic degradation of azo dyes in aqueous solution: kinetic and mechanistic investigations: a review, *Appl. Catal. B. Environ.* 49 (2004) 1–14.

[10] E. Casbeer, V.K. Sharma, X.-Z. Li, Synthesis and photocatalytic activity of ferrites under visible light: a review, *Sep. Purif. Technol.* 87 (2012) 1–14.

[11] D.R. Sulistina, R. Ratnawati, I.W.A. Wiyasa, Rhodamine B increases hypothalamic cell apoptosis and disrupts hormonal balance in rats, *Asian Pac. J. Reprod.* 3 (2014) 180–183.

[12] H. Lee, S.H. Park, Y.-K. Park, B.H. Kim, S.-J. Kim, S.-C. Jung, Rapid destruction of the rhodamine B using TiO₂ photocatalyst in the liquid phase plasma, *Chem. Cent. J.* 7 (2013) 156.

[13] M. Ptaszewska-Koniarsz, J. Goscianska, R. Pietrzak, Removal of rhodamine B from water by modified carbon xerogels, *Colloids Surf. A Physicochem. Eng. Asp.* 543 (2018) 109–117.

[14] H. Abdullah, M.M.R. Khan, H.R. Ong, Z. Yaakob, Modified TiO₂photocatalyst for CO₂ photocatalytic reduction: An overview, *J. CO₂ Util.* 22 (2017) 15–32.

[15] C.B. Ong, L.Y. Ng, A.W. Mohammad, A review of ZnO nanoparticles as solar photocatalysts: Synthesis, mechanisms and applications, *Renew. Sust. Energ. Rev.* 81 (2018) 536–551.

[16] D. Šrbac, C.A. Aggelopoulos, G. Šrbac, M. Dimitropoulos, M. Novaković, T. Ivetić, S.N. Yannopoulos, Photocatalytic degradation of Naproxen and methylene blue: Comparison between ZnO, TiO₂ and their mixture, *Process Saf. Environ. Prot.* 113 (2018) 174–183.

[17] A.L. Linsebigler, G. Lu, J.T. Yates, Photocatalysis on TiO₂ Surfaces: Principles, mechanisms, and selected results, *Chem. Rev.* 95 (1995) 735–758.

[18] A. Zaleska, Doped-TiO₂: a review, *Recent. Pat. Electr. Electron. Eng.* E 2 (2008) 157–164.

[19] S. Liang, K. Xiao, Y. Mo, X. Huang, A novel ZnO nanoparticle blended poly-vinylidene fluoride membrane for anti-irreversible fouling, *J. Membr. Sci.* 394–395 (2012) 184–192.

[20] B. Dindar, S. İçli, Unusual photoreactivity of zinc oxide irradiated by concentrated sunlight, *J. Photochem. Photobio. A Chem.* 140 (2001) 263–268.

[21] N. Daneshvar, D. Salari, A.R. Khataee, Photocatalytic degradation of azo dye acid red 14 in water on ZnO as an alternative catalyst to TiO₂, *J. Photochem. Photobio. A Chem.* 162 (2004) 317–332.

[22] B. Pal, M. Sharon, Enhanced photocatalytic activity of highly porous ZnO thin films prepared by sol-gel process, *Mater. Chem. Phys.* 76 (2002) 82–87.

[23] K.M. Lee, C.W. Lai, K.S. Ngai, J.C. Juan, Recent developments of zinc oxide based photocatalyst in water treatment technology: a review, *Water Resea.* 88 (2016) 428–448.

[24] T. Phongamwong, M. Charoenpanich, J. Limtrakul, Role of chlorophyll in Spirulina on photocatalytic activity of CO₂ reduction under visible light over modified N-doped TiO₂ photocatalysts, *Appl. Catal. B. Environ.* 168 (2015) 114–124.

[25] T. Phongamwong, W. Donphai, P. Prasitchoke, C. Rameshan, N. Barrabéis, W. Klysubun, G. Rupprechter, M. Charoenpanich, Novel visible-light-sensitized Chl-Mg/P25 catalysts for photocatalytic degradation of rhodamine B, *Appl. Catal. B. Environ.* 207 (2017) 326–334.

[26] M. Joshi, S.P. Kamble, N.K. Labhsetwar, D.V. Parwate, S.S. Rayalu, Chlorophyll-based photocatalysts and their evaluations for methyl orange photoreduction, *J. Photochem. Photobio. A Chem.* 204 (2009) 83–89.

[27] P. Kumbhakar, S. Biswas, P. Kumbhakar, Observation of high photocatalytic activity by tuning of defects in chemically synthesized ethylene glycol capped ZnO nanorods, *Optik* 154 (2018) 303–314.

[28] L. Wang, Y. Wu, F. Chen, X. Yang, Photocatalytic enhancement of Mg-doped ZnO nanocrystals hybridized with reduced graphene oxide sheets, *Prog. Nat. Sci. Mater. Int.* 24 (2014) 6–12.

[29] Ş.Ş. Türkyilmaz, N. Güy, M. Özcar, Photocatalytic efficiencies of Ni, Mn, Fe and Ag doped ZnO nanostructures synthesized by hydrothermal method: The synergistic/antagonistic effect between ZnO and metals, *J. Photochem. Photobio. A Chem.* 341 (2017) 39–50.

[30] Q.T.H. Ta, S. Park, J.-S. Noh, Ag nanowire/ZnO nanobush hybrid structures for improved photocatalytic activity, *J. Coll. Interf. Sci.* 505 (2017) 437–444.

[31] S.P. Meshram, P.V. Adhyapak, D.P. Amalnerkar, I.S. Mulla, Cu doped ZnO micro-balls as effective sunlight driven photocatalyst, *Ceram. Int.* 42 (2016) 7482–7489.

[32] A.N. Kadam, T.G. Kim, D.S. Shin, K.M. Garadkar, J. Park, Morphological evolution of Cu doped ZnO for enhancement of photocatalytic activity, *J. Alloys. Compd.* 210 (2017) 102–113.

[33] S.-H. Hsieh, J.-M. Ting, Characterization and photocatalytic performance of ternary Cu-doped ZnO/Graphene materials, *Appl. Surf. Sci.* 427 (2018) 465–475.

[34] C.-M. Chou, Y.-C. Chang, P.-S. Lin, F.-K. Liu, Cu-doped ZnO nanowires as highly efficient continuous-flow photocatalysts for dynamic degradation of organic pollutants, *J. Photochem. Photobiol. A Chem.* 347 (2017) 1–8.

[35] F. Ghahramanifard, A. Rouhollahi, O. Fazlolahzadeh, Electrodeposition of Cu-doped p-type ZnO nanorods; effect of Cu doping on structural, optical and photoelectrocatalytic property of ZnO nanostructure, *Superlatt. Microstruct.* 114 (2018) 1–14.

[36] N. Narayanan, N.K. Deepak, Enhancement of visible luminescence and photocatalytic activity of ZnO thin films via Cu doping, *Optik* 158 (2018) 1313–1326.

[37] M. Ferhat, A. Zaoui, R. Ahuja, Magnetism and band-gap narrowing in Cu-doped ZnO, *Am. Inst. Phys. 94* (2009) 142502.

[38] S. Akir, A. Barras, Y. Coffinier, M. Bououdina, R. Boukherroub, A.D. Omrani, Eco-friendly synthesis of ZnO nanoparticles with different morphologies and their visible light photocatalytic performance for the degradation of Rhodamine B, *Interceram. - Int. Ceram. Rev.* 42 (2016) 10259–10265.

[39] A. Bennett, L. Bogorad, Complementary chromatic adaptation in a filamentous blue-green Algae, *J. Cell Biol.* 58 (1973) 419–435.

[40] M. Ebrahimi, S. Yousefzadeh, M. Samadi, C. Dong, J. Zhang, A.Z. Moshfegh, Facile preparation of branched hierarchical ZnO nanowire arrays with enhanced photocatalytic activity: A photodegradation kinetic model, *Appl. Surf. Sci.* 435 (2018) 108–116.

[41] A. Šutka, T. Käämbre, R. Pärna, I. Juhnevica, M. Maiorov, U. Joost, V. Kisand, Co doped ZnO nanowires as visible light photocatalysts, *Solid State Sci.* 56 (2016) 54–62.

[42] K.V. Kumar, K. Porkodi, A. Selvaganapathi, Constrain in solving Langmuire-Hinshelwood kinetic expression for the photocatalytic degradation of Auramine O aqueous solutions by ZnO catalyst, *Dyes Pigm.* 75 (2007) 246–249.

[43] X. Chen, H. Zhang, D. Zhang, Y. Miao, G. Li, Controllable synthesis of mesoporous multi-shelled ZnO microspheres as efficient photocatalysts for NO oxidation, *Appl. Surf. Sci.* 435 (2018) 468–478.

[44] Y.-R. Kang, J. Park, S.K. Jung, Y.H. Chang, Synthesis, characterization, and functional properties of chlorophylls, pheophytins, and Zn-pheophytins, *Food Chem.* 245 (2018) 943–950.

[45] Z. Mehraban, F. Farzaneh, A. Shafeekhani, Synthesis and characterization of a new organic-inorganic hybrid NiO-chlorophyll-a as optical material, *Opt. Mater. Express* 29 (2007) 927–931.

[46] C. Pholnak, C. Sirisathitkul, D.J. Harding, Characterizations of octahedral zinc oxide synthesized by sonochemical method, *J. Phys. Chem. Solids* 72 (2011) 817–823.

[47] W. Hu, F. Wu, W. Liu, J. Liu, Nitrate-induced photodegradation of colorants and the corresponding mechanism study, *J. Adv. Oxid. Technol.* 21 (2018) 285–296.

[48] S. Muralidharan, R.G. Hayes, Intense satellites in the N 1s x-ray photoelectron spectra of certain metalloporphyrins, *J. Am. Chem. Soc.* 102 (1980) 5106–5107.

[49] M.N. Lyulyukin, A.S. Besov, A.V. Vorontsov, Acetone and ethanol vapor oxidation via negative atmospheric coronadischarge over titania-based catalysts, *Appl. Catal. B. Environ.* 183 (2016) 18–27.

[50] H.L. Yan, X.L. Zhong, J.B. Wang, G.L. Huang, S.L. Ding, G.C. Zhou, Y.C. Zhou, Cathodoluminescence and room temperature ferromagnetism of Mn-doped ZnO nanorod arrays grown by chemical vapor deposition, *Appl. Phys. Lett.* 90 (2007) 082503.

[51] R.B. Liu, A.L. Pan, H.M. Fan, F.F. Wang, Z.X. Shen, G.Z. Yang, S.S. Xie, B.S. Zou, Phonon-assisted stimulated emission in Mn-doped ZnO nanowires, *J. Phys. Condens. Matter* 19 (2007) 136206.

[52] K. Vanheusden, W.L. Warren, C.H. Seager, D.R. Tallant, J.A. Voigt, Mechanisms behind green photoluminescence in ZnO phosphor powders, *J. Appl. Phys.* 79 (1996) 7983.

[53] A. Cai, L. Du, Q. Wang, Y. Chang, X. Wang, X. Guo, Kelp-inspired N-I-doped ZnO photocatalysts with highly efficient catalytic activity, *Mater. Sci. Semicond. Process.* 43 (2016) 25–33.

[54] L. Liu, H. Ou, K. Hong, L. Wang, Evidence of a strong electronhole separation effect in ZnO@TiO₂ core/shell nanowires, *J. Alloys. Compd.* 749 (2018) 217–220.

[55] S. Choi, J.Y. Do, J.H. Lee, C.S. Ra, S.K. Kim, M. Kang, Optical properties of Cu-incorporated ZnO (Cu_xZn_{1-x}O) nanoparticles and their photocatalytic hydrogen production performances, *Mater. Chem. Phys.* 205 (2018) 206–209.

[56] A. Kathiravan, M. Chandranohan, R. Renganathan, S. Sekar, Cyanobacterial chlorophyll as a sensitizer for colloidal TiO₂, *Spectrochim. Acta Part A Mol. Biomol. Spectrosc.* 71 (2009) 1783–1787.

[57] M.P. Suryawanshi, S.W. Shin, U.V. Ghorpade, K.V. Gurav, C.W. Hong, G.L. Agwane, S.A. Vanalakar, J.H. Moon, J.H. Yun, P.S. Patil, J.H. Kim, A.V. Moholkar, Improved photoelectrochemical performance of Cu₂ZnSnS₄(CZTS) thin films prepared using modified successive ionic layer adsorption and reaction (SILAR) sequence, *Electrochim. Acta* 150 (2014) 136–145.

[58] D.W. Lawlor, Photosynthesis: Molecular, Physiological and Environmental Process, second ed., Longman Scientific & Technical, Essex, 1993, pp. 1–8.

[59] M.F. Hopkins, N.R. Baker, Photosynthesis: Energy Transduction: A Practical Approach, IRL Press Limited, Oxford, Washington D.C, 1986, pp. 1–15.

[60] I.-H. Tseng, J.C.-S. Wu, Chemical states of metal-loaded titania in the photo-reduction of CO₂, *Catal. Today* 97 (2004) 113–119.

[61] S. Xu, J. Ng, Y. Wang, A.J. Du, D.D. Sun, Simultaneous copper ion removal and hydrogen production from water over a TiO₂ nanotube photocatalyst, *Water Sci. Technol.* 65 (2012) 533–538.